Int. J. Heat Mass Transfer. Vol. 29, No. 10, pp. 1593–1604, 1986
Printed in Great Britain

0017-9310/86 $3.00 + 0.00
Pergamon Journals Ltd.

Enclosed gas and liquid with nonuniform heating from above

S. K. AGGARWAL,* J. IYENGAR† and W. A. SIRIGNANO‡

* Department of Mechanical Engineering, University of Illinois, Chicago, IL 60680, U.S.A.
† Westinghouse Electric Corporation, Pittsburgh, PA 15230, U.S.A.
‡ Department of Mechanical Engineering, University of California, Irvine, CA 92717, U.S.A.

(*Received* 1 *November* 1985 *and in final form* 19 *May* 1986)

Abstract—Buoyancy-driven flows of gases above liquids in a common enclosure with nonuniform heating from above are studied via finite-difference solutions of the governing equations. Unsteady solutions are calculated and steady-state solutions are sought as asymptotes. Grashof numbers between 10^3 and 10^8 are examined and multicellular circulatory flow structure is found at the higher Grashof numbers. Convective transport dominates for higher Grashof numbers while conductive transport is the primary mechanism at the lower Grashof numbers. Surface tension has a major effect upon the gas flow field only at lower Grashof numbers but since conduction dominates there, it does not significantly affect transport.

INTRODUCTION

WITH the advent of space flight and particularly with the controlled-gravity opportunities provided by the Space Shuttle flights, there has been a renewed interest in studying the influence of gravity and surface-tension forces on fluid motions and combustion processes. A comprehensive review on this subject is provided by Ostrach [1]. In the present paper, the focus is on investigating, via finite-difference calculations, the influence of these forces on the ignition of a liquid-fuel pool and the fluid motions generated during these processes. Fuel vaporization and chemical reaction are not considered in this first analysis. Only fluid motion and heat transport are examined. The gravity affects these processes in several ways. Consider, for example, an enclosed cavity partially filled with a liquid fuel. When an ignition source is brought near the top of the cavity, due to nonuniform heating from above, gravity induces convective motions in the gas medium which influences the heat transfer process in the cavity. The gravity also determines the hydrostatic pressure distribution in the cavity. The gas motion in the ullage induces liquid motion through shear forces at the interface. The liquid motion is also generated by gravity due to nonuniform heating. Surface tension varies along the liquid–gas interface due to the variation of temperature and composition. Note only temperature variations are presently considered since fuel vaporization is not included. The surface tension gradient generates flow motions. The effects of surface-tension-driven flows in liquid-fuel pool fires has been discussed by Sirignano [2], Sirignano and Glassman [3], and Torrance [4]. The relative magnitude of these motions will depend on the magnitudes of gravity and surface-tension gradients. In particular, certain nondimensional groupings will be shown to contain these important parameters. In this paper, the above processes have been studied numerically by solving the governing equations by finite-difference methods. The governing equations and the numerical procedure are described in the following two sections. The results are presented in the last section.

‡ Address correspondence to: W. A. Sirignano, Office of the Dean, School of Engineering, University of California, Irvine, CA 92717, U.S.A.

THE GOVERNING EQUATIONS

The governing equations for the present case are the incompressible unsteady Navier–Stokes equations along with an appropriate energy equation for two-dimensional flow. The Boussinesq approximation is employed to include the buoyancy effects in the momentum equations. The nondimensional equations in terms of the primitive variables are:

Continuity equation

$$\frac{\partial v}{\partial y}+\frac{1}{x^a}\frac{\partial}{\partial x}(x^a u)=0. \tag{1}$$

Momentum equation in y (axial) direction

$$\frac{\partial v}{\partial t}+\frac{\partial v^2}{\partial y}+\frac{\partial uv}{\partial x}+a\frac{uv}{x}=-E\frac{\partial p_e}{\partial y}+\frac{G_r}{Re^2}T + \frac{1}{Re}\left(\frac{\partial^2 v}{\partial y^2}+\frac{1}{A^2}\frac{\partial^2 v}{\partial x^2}+\frac{a}{A^2}\frac{1}{x}\frac{\partial v}{\partial x}\right). \tag{2}$$

Momentum equation in x (radial) direction

$$\frac{\partial u}{\partial t}+\frac{\partial uv}{\partial y}+\frac{\partial u^2}{\partial x}+a\frac{u^2}{x}=-\frac{E}{A}\frac{\partial p_e}{\partial x}+\frac{1}{Re}\left[\frac{\partial^2 u}{\partial y^2}+\frac{1}{A^2}\frac{\partial^2 u}{\partial x^2} + \frac{a}{A^2}\left(\frac{1}{x}\frac{\partial u}{\partial x}-\frac{u}{x^2}\right)\right]. \tag{3}$$

NOMENCLATURE

a	coordinate parameter, $a = 0$ for planar, $a = 1$ for axisymmetric coordinates	T_0'	initial temperature in the cavity [K]
		T_w'	hot body temperature [K]
		T	normalized temperature, $(T' - T_0')/(T_w' - T_0')$
A	L/H		
E	$p_0'/\rho_0' u_0'^2$	u'	velocity in x (radial) direction, $uu_0'L/H$ [cm s^{-1}]
Gr	Grashof number, $g\beta(T_w' - T_0')H^3/\nu'^2$		
G_{rr}	$G_r/R_e^2 = g\beta(T_w - T_0)H/u_0'^2$	V'	velocity in y (axial) direction, VU_0'
g	gravitational acceleration [cm s^{-2}]	u_0'	reference velocity [cm s^{-1}]
H	cavity height [cm]	x'	distance in x direction, xL
k_r	ratio of liquid and gas thermal conductivities	y'	distance in y direction, yH.
L	one-half of cavity length [cm]		
p'	thermodynamic pressure	Greek symbols	
p_s'	static pressure	α'	thermal diffusivity [cm^2 s^{-1}]
p_e'	$p' - p_s'$	β	thermal expansion coefficient, $-(1/\rho)(\partial\rho/\partial T)_p$
p_e	p_e'/p_0'		
p_0'	reference pressure for normalization	μ_r	ratio of liquid and gas viscosities
Pr	Prandtl number, ν'/σ'	ν'	kinematic viscosity [cm^2 s^{-1}]
Re	Reynolds number, $u_0'H/\nu'$	ρ_0'	reference density [g cm^{-3}]
t'	time variable(s), tH/u_0'	σ'	reference value of surface tension
T'	dimensional temperature [K]	σ	nondimensional surface tension.

Energy equation

$$\frac{\partial T}{\partial t}+\frac{\partial vT}{\partial y}+\frac{\partial uT}{\partial x}+a\frac{uT}{x} = \frac{1}{RePr}\left(\frac{\partial^2 T}{\partial y^2}+\frac{1}{A^2}\frac{\partial^2 T}{\partial x^2}+\frac{a}{A^2}\frac{1}{x}\frac{\partial T}{\partial x}\right). \quad (4)$$

The assumptions used in writing these equations are that the transport coefficients are constant and that the viscous dissipation is negligible.

The coordinate system is shown in Fig. 1. The equations are written in a general form so that they are applicable in planar ($a = 0$) as well as in axisymmetric ($a = 1$) coordinates. All results presented herein are for the axisymmetric configuration. The normalization procedure is given in the nomenclature. The dimensional variables are generally indicated by a prime. u_0', p_0', L and H are respectively the reference velocity, the reference pressure, and the reference lengths in x (radial) and y (axial) directions employed for normalization. The reference time is obtained from u_0' and H. The temperature is normalized by using the hot wall temperature T_w' and the cold wall temperature (also the initial temperature in the cavity) T_0'. Note that the pressure p_e' is the difference between the actual pressure p' and the static pressure of the medium p_s'. The above normalization gives rise to the following dimensionless groups: A, E, Gr, Re and Pr, which are respectively the aspect ratio of two reference lengths (L/H), the Euler number, the Grashof number based upon H, the Reynolds number based on u_0' and H, and the Prandtl number.

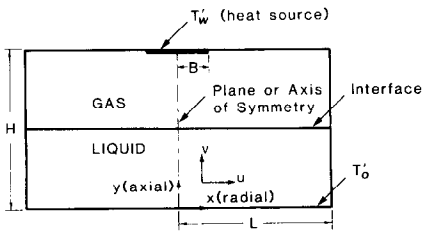

FIG. 1. Physical model for the effect of gravity on motion in liquid pool and gas ullage.

It is important to note that equations (1)–(4) are applicable to the gas phase as well as to the liquid phase. Of course, the values of dimensionless groups are different for the two phases on account of property differences.

The initial conditions correspond to two quiescent fluids in a cavity with the air being heated nonuniformly from above. The initial temperature in the cavity is 300 K everywhere except for a hot region at the cavity top. The radius of the hot region is one-fifth of the cavity radius. It is noteworthy that, initially, our focus was on the two-fluid case. However, the results, discussed in a later section, generate enough interest and questions for considering the one-fluid case in detail.

The boundary conditions

No-slip velocity conditions are applied at the top wall ($y = 1$), side wall ($x = 1$), and bottom wall ($y = 0$). For $0 \leqslant x \leqslant 0.2$, $T = T_w$ at the top wall with adiabatic conditions on the remainder of the top wall and on the

side wall. $T = 0$ at the bottom wall. Symmetry conditions are applied at $x = 0$.

The interface conditions

In the present calculations, the location of the gas–liquid interface is assumed to be known and is given by $y = y_I$. For most of the results $y_I = 0.5$. The thermal and hydrodynamic conditions which must be satisfied at the interface are:

$$T_l = T_g$$

$$k_r\left(\frac{\partial T}{\partial y}\right)_l = \left(\frac{\partial T}{\partial y}\right)_g \tag{5}$$

$$v = 0$$

$$u_l = u_g$$

$$\mu_r\left(\frac{\partial u}{\partial y}\right)_l = \left(\frac{\partial u}{\partial y}\right)_g + N\frac{\partial \sigma}{\partial T}\frac{\partial T}{\partial x} \tag{6}$$

where

$$N = \sigma'/Au_0'\mu_g'$$

and μ_r is a ratio of liquid viscosity to gas viscosity and $\sigma' \equiv (\partial\sigma'/\partial T')\Delta T'$. A boundary-layer thickness δ' exists on the gaseous side of the interface whereby we can estimate that

$$\frac{\delta'}{L} = (Re_g)^{-1/2}$$

where Re_g is the Reynolds number based on the gas properties. This might underestimate the thickness in some cases since the velocity near the surface can be much less than the characteristic velocity.

Depending on the dominant forces, the Reynolds number may be related to a Grashof number or to a surface-tension Reynolds number [1]. The non-dimensional velocity gradient $(\partial u/\partial y)_g$ is expected to be of order $Re_g^{1/2}/A$ at the surface. N must be of this same order if surface tension were important at the surface.

Note that the term N can be related to the Marangoni number (a parameter used in surface-tension-driven flows) which is defined as

$$Ma = \frac{\sigma_T \Delta T H}{\mu_g' \alpha'}$$

where

$$\sigma_T = \frac{d\sigma}{dT}.$$

Then one can obtain

$$\frac{M_a}{N} = \frac{Lu_0'}{\alpha'}.$$

In other words, the ratio is a Péclet number.

THE NUMERICAL METHOD

The starting point for the numerical computations was an existing code 'SOLA' which has been developed at Los Alamos Laboratory [5]. The code solves the incompressible, unsteady Navier–Stokes equation in two-dimensional planar or axisymmetric coordinates. A finite-difference, staggered-grid scheme is employed to solve the two momentum equations. The numerical scheme is semi-implicit in the sense that the pressure is treated implicitly. Thus the explicit stability criterion for the convective terms is based on the maximum fluid velocity rather than on the speed of sound. First, the values of two velocity components are predicted by using the velocity and pressure values at the known time step. Then the pressure and velocities are corrected iteratively until the continuity equation is satisfied within a specified accuracy. A parameter is employed to control the amount of donor-cell or upwind differencing. For complete upwind differencing, the above parameter is unity, whereas for complete center differencing it is zero. For the present calculations, a minimum value of 0.5 was required to avoid numerical oscillations.

The major modifications in the 'SOLA' code are in the inclusion of buoyancy terms (through a Boussinesq approximation) in the momentum equations, and a solver for the energy equation; note that all the equations are coupled due to the buoyancy term. Modifications were also needed to solve the buoyancy-driven flow in two fluids with an interface. For the problem considered here the interface is well defined, has no curvature, and is invariant with time. The surface-tension-gradient effects in the interface hydrodynamic boundary conditions are also included.

Computational cells in the gas and liquid phases across the interface are constructed so that the temperature is defined in the cell center whereas the velocity u is defined at the cell boundary. Two fictitious values of temperature and of velocity are used in writing the finite-difference form of the interface conditions. Then the thermal interface conditions (5) can be expressed as

$$T_l + \bar{T}_l = T_g + \bar{T}_g$$

$$k_r(\bar{T}_l - T_l) = (T_g - \bar{T}_g)$$

where a bar indicates a fictitious quantity. The step size Δy is assumed to be the same in the gas and liquid phases.

Similarly, the hydrodynamic interface conditions (6) can be finite-differenced, at the right-hand boundary of the cell as

$$u_l + \bar{u}_l = u_g + \bar{u}_g$$

$$\mu_r(\bar{u}_l - u_l) = (u_g - \bar{u}_g) + B$$

where $B = N(d\sigma/dT)(\partial T/\partial x)\Delta y$ is to be computed at the interface location which is at the right-hand boundary of the cell.

RESULTS

A schematic of the general configuration employed in the calculations is shown in Fig. 1. The base

calculations presented here are for a cavity height of 10 cm and a cavity diameter of 20 cm. The cavity aspect ratio, which is the ratio of radius to height, is unity. This aspect ratio is varied in some of the other calculations. The results are obtained for a range of Grashof numbers from 10^3 to 10^8 for the two-fluid case as well as for the one-fluid case. In the base calculations for the two-fluid case, the liquid surface height is one-half of the cavity height. This height ratio is also varied. For a given set of calculations, the Grashof number is specified. As established by the order of magnitude analysis (of the type shown in the Appendix), at one g and at $\Delta T > 1000$ K the dominant mechanism is expected to be buoyancy. Consequently for the case without surface tension or with weak surface tension effects, the reference velocity is obtained by equating the coefficient of buoyancy terms [see equation (2)], which is the ratio of Grashof number of the Reynolds number squared, to unity. In other words, the reference velocity is obtained by balancing the buoyancy and the inertia terms. It is also noteworthy that the reference velocity is based on the gas properties since the gas motion is initiated first. The hot wall temperature (T'_w) is also calculated by employing the gas properties and the relation

$$Gr = \frac{g\beta(T'_w - T'_0)H^3}{\nu'^2}.$$

Other gas properties for the present calculations are given in Table 1. Note that the reference pressure is calculated after specifying the Euler number, the density, and the reference velocity, which is calculated, as discussed above, by specifying the Grashof number. The liquid properties are also given in Table 1. The Euler number for the liquid phase is obtained from the reference pressure and the reference velocity, as calculated above, and the liquid density. The liquid Reynolds number, which is required in equations (2) and (3), is also based on the same reference velocity.

Table 1

I. Gas properties
Kinematic viscosity $= \nu' = 0.20\,\text{cm}^2\,\text{s}^{-1}$
Density $= \rho' = 1.17 \times 10^{-3}\,\text{g cm}^{-3}$
Prandtl number $= Pr = 0.7$
Coefficient of thermal expansion $= \beta = 1/T'_0 = 0.00334\,\text{K}^{-1}$
Euler number $= E = 1.0$
Specific heat at constant pressure $= C_p = 0.25\,\text{cal g}^{-1}\,\text{K}^{-1}$
II. Liquid properties
$\nu' = 0.07\,\text{cm}^2\,\text{s}^{-1}$
$\rho' = 1.0\,\text{g cm}^{-3}$
$Pr = 10.0$
$\beta = 0.001\,\text{K}^{-1}$
$C_p = 0.7\,\text{cal g}^{-1}\,\text{K}^{-1}$

The parameter G_{rr}, the ratio of Grashof number and Reynolds number squared, for the liquid-phase equations is obtained by multiplying the G_{rr} for the gas and the ratio of thermal expansion coefficients of liquid and gas.

Most of the present results have been obtained for a 20×20 mesh which gives a value of 0.05 for both Δx and Δy. The time-step size is 0.02 seconds. When this value is decreased by a factor of two, it is observed that the results change by less than one percent for the low Grashof number of 10^3 but differences become larger as Grashof number increases. Note that the dimensionless time-step size depends upon the Grashof number. The value of the convergence criterion is 2×10^{-4} and the value of the over-relaxation factor is 1.7. The value of the upwind-differencing parameter is 0.9 which means that numerical diffusion is present especially for higher Grashof numbers.

One-fluid case

The one-fluid case has been investigated by numerous researchers in the past [1, 6, 7]. However, the particular case of nonuniform heating from above, the subject of this investigation, has not been treated before. The results, presented in terms of temperature contours and velocity vector plots at different times, have been obtained for Grashof numbers of 10^4, 10^5, 10^6 and 10^8. For these results, the Prandtl number is 0.7. The fluid, which is initially quiescent, is air.

Figure 2 gives the temperature contours at 80 s for $Gr = 10^4$. The calculations have been performed up to a t (nondimensional time) value of 16. Note the characteristic time, based on the reference velocity and the cavity height, for this case is 5 s. The maximum nondimensional velocity for this case is about 0.07. Based on this velocity, the time to go around the cavity once will be more than 70 s. But even at 80 s, the temperature contours do not indicate a steady-state situation. No steady state was observed during the time duration of computations. In the two-phase calculations discussed later, where calculations were

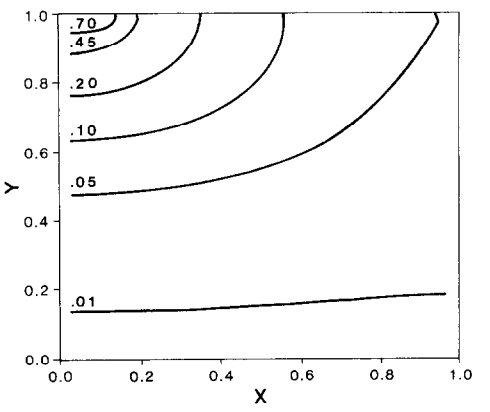

FIG. 2. One-fluid case, $Gr = 10^4$, temperature contours, time: 80 s.

made for longer times, steady states were obtained. The main thrust of this research relates to the two-phase case so extensive calculations were not made in the one-phase case. It is believed that steady states should exist in the one-phase case as well. The attainment of steady state can be detected by computing the total enthalpy (H_T) in the cavity as a function of time. H_T for the axisymmetric case is defined as

$$H_T = \int_y \int_x C_p T x \, dx \, dy$$

where C_p and T are dimensionless. A plot of H_T vs the nondimensional time t (not shown here) clearly indicates that a steady state is not achieved at this time.

The comparison of temperature contours of Fig. 2 to those for $Gr = 0$ (not shown) indicates that the heat transfer mechanism is predominantly conduction. Thus, the effect of natural convection is relatively small for $Gr = 10^4$. The characteristic diffusion time based on the cavity height and thermal diffusivity is 350 s, which should also be the order of magnitude of the time for attaining the steady-state conditions.

The velocity vector plots at different times for this case (not shown) indicate that circulatory motion is established initially near the hot region. At later times the circulatory cell moves lower and to the right in the cavity. The important observation is that there is unicellular motion in the cavity for $Gr = 10^4$.

The results for $Gr = 10^5$ are qualitatively similar to the previous case but are not shown here.

The results for $Gr = 10^6$ are quite different from those of the previous two cases, in that the natural convective heat transfer is dominant and in that the secondary flow is observed.

At 15 s, the secondary flow is started near the bottom right-hand corner of the cavity. At 20 s, the secondary cell is clearly established. The generation of the secondary cell may be explained by the thermal gradients which are established in the lower part of the cavity. The first cell is established by buoyancy effects when the air in the top center of the enclosure is hotter than the air at the side of the enclosure. This horizontal temperature (and therefore density) gradient starts the motion. Similarly, at higher Grashof number when convection dominates, the air at some lower height becomes hotter on the side than in the center. Then a secondary cell starts due to buoyancy with opposite circulation to the first cell. The same mechanism can produce more cells with alternating direction if Grashof number is sufficiently high.

As the Grashof number is increased further, the above effect intensifies. This is clearly demonstrated by the results at $Gr = 10^8$ in Figs. 3 and 4. The effect of buoyancy is much stronger and the thermal gradients for generating the secondary cell are established much earlier. The secondary cell appears at 2.5 s. The number of cells increases with time. For example at 20 s, which is 400 times the characteristic time, there are five cells as shown in Fig. 3. It should be noted, however, that except for the first two cells near the cavity top, the velocities are quite small. For example, the maximum velocity in the second cell (counting from top) is 0.45 of that in the first one. For the third cell, it is only 0.03 of that in the first cell, whereas in the fourth and fifth cells the velocities are minuscule. At some point in time, because additional cells have smaller velocity and smaller size, conduction within the lowest cell becomes as important as convection. Then the horizontal gradient of temperature does not reverse its sign and buoyancy will not cause further formation of new cells. In Fig. 4, the temperature contours indicate that convection dominates conduction in this case at that time. It is also noteworthy that for each rotating cell, there are only three to four grid points in the y direction. Thus for the case of $Gr = 10^8$, the spatial resolution may not have been sufficient. However, poor resolution would not

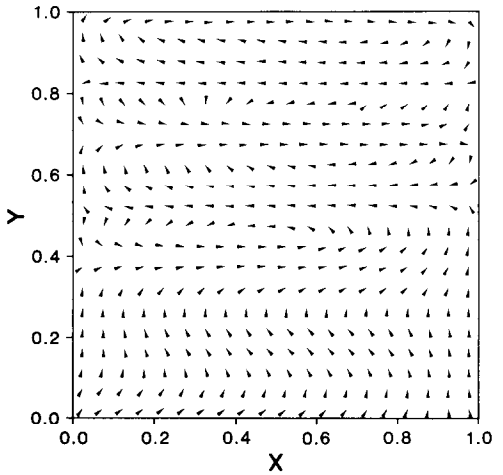

FIG. 3. One-fluid case, $Gr = 10^8$, velocity vector plots, time: 20 s.

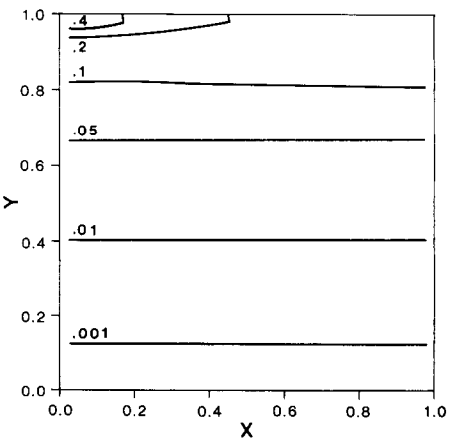

FIG. 4. One-fluid case, $Gr = 10^8$, temperature, time: 20 s.

lead to the artificial creation of additional circulatory cells. On the contrary, it can only mask their presence due to an artificial dissipation caused by a numerical viscosity effect.

The major conclusion from the results, presented so far, is that for a nonuniformly heated cavity from above, as the Grashof number is increased, the unicellular motion degenerates into multicellular motion; the number of cells is a function of Grashof number and time.

The issue of multicellular motions in the buoyancy-driven cavity flow remains not completely understood in the literature. Secondary cells have been observed by Emara and Kulacki [8] and by Ostrach *et al.* [9]. Ozoe *et al.* [6] also observed a series of roll cells with axes parallel to each other and perpendicular to the long axis of the channel with the channel being horizontal or inclined up to a critical angle and the hot side below. However, any generalization or direct comparison with these results is not possible due to the difference in configurations and boundary conditions. For example, Emara and Kulacki [8] studied the natural convection in a rectangular cavity with uniform heating of the fluid with adiabatic left, bottom and right walls and an isothermal top wall. In their study involving heat generation in the fluid, as Rayleigh number is increased, unicellular motion first breaks into two and then into four cells. In the experimental results of Ostrach *et al.* [9] for a range of aspect ratio, Grashof number and Prandtl number, the secondary cells were observed near the enclosure ends for certain values of aspect ratio and Rayleigh number.

It is also noteworthy that in the present case we could generate unicellular motion even at high Grashof number by using different thermal boundary conditions. For the case when there is nonuniform heating from above but with top, right and bottom walls being isothermal and the left side being the axis of the system, a secondary cell was observed at $Gr = 1.6 \times 10^7$ but not at significantly lower values. With isothermal walls, less heat is transported to the lower regions of the cavity and the effects of buoyancy are limited to a smaller domain. It is believed that this explains the difference in the number of cells as compared to the adiabatic case.

Two-fluid case without surface tension

Now we will discuss the two-fluid case; the enclosure is partially filled with liquid at the bottom and the rest is filled with gas.

The effect of varying the Grashof number (Gr) is studied, keeping all other variables fixed. Hence variations in surface tension are neglected. The effects of surface tension are considered in the next section. The aspect ratio (the ratio of cavity radius to cavity height) and the acceleration due to gravity (g), are fixed at unity and 981 cm s^{-2}, respectively. The interface is located at the center of the cavity for these initial calculations. The results are obtained for Gr equal to 10^4, 10^5 and 10^7. Note that the Grashof number is still calculated using the total height of the enclosure; a Grashof number calculated based upon the gas height or upon the liquid height would be lower by a factor of eight. There is no need without surface tension effects to specify the temperature difference independently of the Grashof number, in order to calculate the nondimensional solution. The reference velocity will also be independent of the temperature difference.

The calculations for $Gr = 10^5$ (see Fig. 5) show a unicellular motion in the gas phase at all times. (Calculations were made up to 60 s.) As observed in the one-fluid case, the gas is heated near the hot surface and expands radially. A clockwise eddy is generated in the gas phase and the center of the circulatory motion is seen to move to the right as time increases. It is also observed that after 25 s, the center of the circulatory motion is established and does not move further to the right. Although the profiles look alike after this time, steady state has not been reached. The attainment of steady state is discussed below.

It is also found that a unicellular motion starts to form in the liquid phase and is established by about 25 s. Comparing the results for $Gr = 10^4$, we observe the unicellular motion in the gas phase and liquid phase as before, except the center of the circulatory motion is now slightly towards the left. This is an indication of the reduced buoyancy effect.

For $Gr = 10^7$ as shown in Fig. 6, two cells are eventually seen in the gas-phase motion. At time 5.0 s, only one cell is observed, but at time 10.0 s and later there are two cells observed in the gas phase and a single cell in the liquid phase. This indicates the strong effect due to buoyancy. The temperature contours for $Gr = 10^4$ and 10^5 indicate that the effect of natural convection is relatively small and the temperature

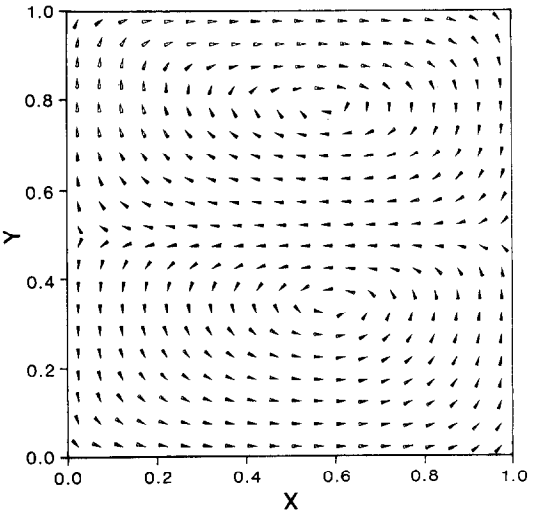

FIG. 5. Two fluids without surface tension, $Gr = 10^5$, $h_1/h = 0.5$, velocity vector plots, time: 60 s.

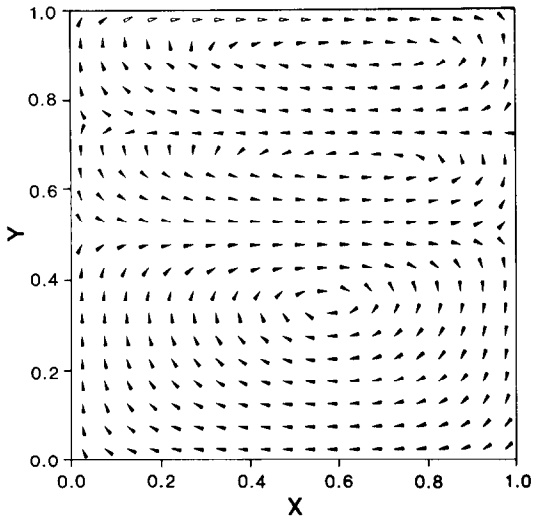

FIG. 6. Two fluids without surface tension, $Gr = 10^7$, $h_1/h = 0.5$, velocity vector plots, time: 60 s.

patterns (see Fig. 7) are similar to those for pure conduction. For $Gr = 10^7$, as shown in Fig. 8 the effect due to convection can be seen, which indicates the influence of buoyancy on the motion.

The results must be calculated for a sufficient time to obtain the steady state. The plot of total enthalpy vs time for $Gr = 10^5$ is presented here (Fig. 9). It should be noted that the rate of change of total enthalpy decreases as time increases, thus indicating the approach of steady state. In order to reach the steady state, calculations were performed up to 200 s. The time step Δt was now increased to 0.1 s. This figure shows that the total enthalpy remains constant after about 160 s. This indicates the attainment of steady state. As Grashof number increases and the number of circulatory cells increases, the time to reach steady state decreases. Essentially the conduction time across stream surfaces within each cell is a controlling factor.

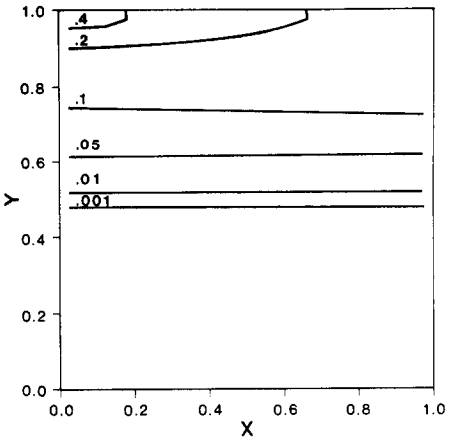

FIG. 8. Two-fluid case without surface tension, $Gr = 10^7$, $h_1/h = 0.5$, temperature, time: 60 s.

Two-fluid case with surface tension

The next step in our calculations is the inclusion of surface tension effects at the interface between the gas and liquid. The reference velocity for the nondimensionalization is calculated as indicated by Ostrach [1]. This is shown in the Appendix.

The nondimensional variable N is first calculated to estimate the order of magnitude of the surface-tension effect. A value of -0.1 dyne cm^{-1} K^{-1} for the surface-tension gradient term $\partial\sigma/\partial T$ is used here. This value is typical for liquid hydrocarbons. It should be noted that as the temperature difference $(T_w' - T_0')$ increases, the rate of increase of Gr is less than the rate of increase of the square of the reference velocity. Thus, the Gr/Re_g^2 ratio is decreased. Therefore, surface tension variations become more important than buoyancy as temperature difference increases.

A temperature difference $(T_w' - T_0')$ here in these calculations of 1223 K produces $Gr = 10^8$ at earth gravity. The calculations are performed with this value of $(T_w' - T_0')$ for various values of Gr and g. One could question the validity of the Boussinesq approximation

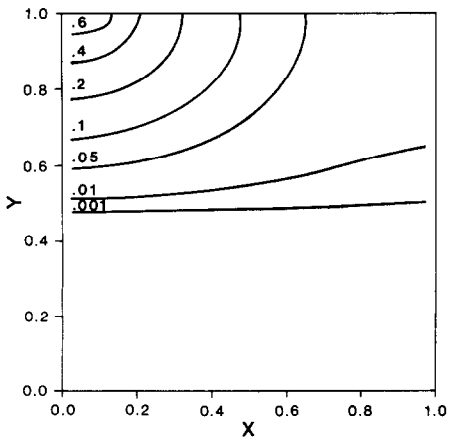

FIG. 7. Two fluids without surface tension, $Gr = 10^4$, $h_1/h = 0.5$, temperature, time: 60 s.

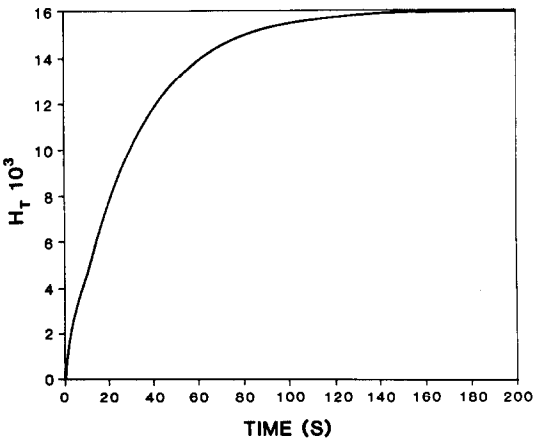

FIG. 9. Two-fluid case without surface tension, $Gr = 10^5$, $h_1/h = 0.5$, nondimensional total enthalpy vs time.

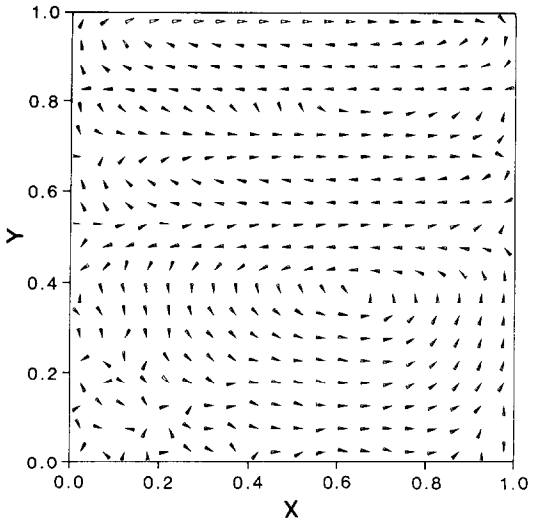

FIG. 10. $Gr = 10^8$, $h_1/h = 0.5$, velocity vector plots with surface tension, time: 60 s.

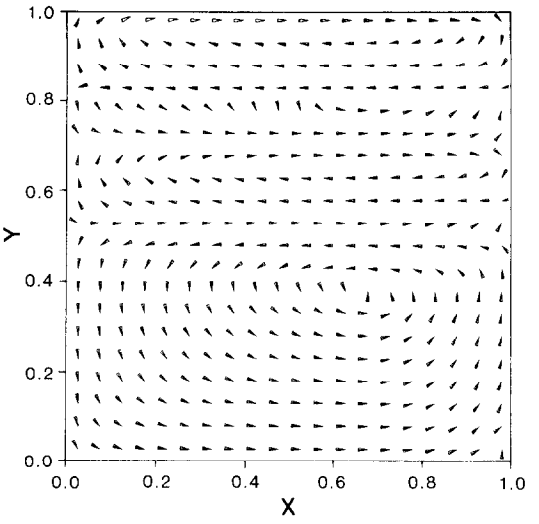

FIG. 11. $Gr = 10^8$, $h_1/h = 0.5$, velocity vector plots without surface tension, time: 60 s.

at these large temperature differences, which are relevant to combustion-related problems. Although some quantitative difficulties result, the approximation still gives qualitatively useful results. Of course, the calculations would apply to other cases with the same value of Gr and N. For example, with a lower temperature difference and properly modified values of length, aspect ratio and gravity, the same values of the similarity parameters would result.

Normally, a surface-tension-related nondimensional parameter such as surface-tension Reynolds number would be reported for these calculations. However, the unknown surface temperature variations are orders of magnitude less than the known temperature difference across the enclosure. Therefore, nondimensional parameters based upon the known temperature difference are very misleading. Note also that different reference velocities result between the cases with and without surface tension. For this reason, dimensional velocities are directly compared between these two cases.

The velocity plots (Figs. 10 and 11) for $Gr = 10^8$, $g = 1.0$ show a great similarity in the velocity vector between the cases with surface tension and the case with no surface tension. Table 2 indicates the comparison in the magnitude of the velocity between the two cases. The plot at 60.0 s, with surface tension shows a fluctuation in the velocity vectors at the bottom left corner in the liquid phase, but the velocities here are very low as compared to the gas-phase velocities. It is assumed that these fluctuations are due to small numerical errors and that we may consider the flow in that region as stagnant. In both cases with and without surface tension there is a unicellular motion in the liquid phase and four cells are noticed in the gas phase. This is due to the high Gr.

Results are also obtained for $Gr = 10^7$, 10^6 and 10^3 with $g = 10^{-1}$, 10^{-2} and 10^{-5}, respectively. For $Gr = 10^7$, the disturbance in the liquid-phase velocity vector, indicated before is seen at earlier times (20.2 s). The reduced value of Gr, results in two cells in the gas phase. $Gr = 10^6$ differs from the $Gr = 10^7$ case, in that only a unicellular motion is present in the gas phase.

Reducing Gr to 10^3 and g to 10^{-5} we observe the interesting results of Figs. 12 and 13, which indicate that there is a relatively strong influence of surface tension. Again, there is a great amount of variation in the velocity vector plots in the lower left corner of the liquid phase. As Table 3 demonstrates, the liquid velocities are very small and the zone with the velocity vector variations may be considered as stagnant. Note that surface tension does cause significant differences in gas phase velocities as well as in liquid phase velocities especially near the interface. At 40.0 s a unicellular motion is seen to start forming and this is also noticed at 60.0 s. The reduced gravity effect influences the flow and allows the surface tension effect to dominate. The temperature profiles with and without surface tension are essentially identical at low Grashof numbers in spite of the differences in velocity profiles. Since conduction dominates, the difference in convective augmentation is insignificant.

A set of calculations with $Gr = 10^8$, $g = 1.0$ and 20×30 mesh is made to study the effect at the interface. The calculations are compared to the case with a 20×20 mesh, to check for accuracy. Gas-phase velocities differed by about 4% at early times. Temperature and liquid-phase velocities differed by about 20–25% at early times but agreement improved to within 6% for temperature at later times. Qualitative agreement is always found with regard to flow direction and the sign of gradients.

The results indicate that for $Gr = 10^8$, 10^7 and 10^6, there is very slight or no difference at all in both gas and liquid phase with and without surface tension. However, when the Gr is reduced to 10^3 and g to 10^{-5},

Table 2. Horizontal velocity profile at mid-radius. $Gr = 10^8$, $g = 1$, $h_1/h = 0.5$, $A = 1$

Vertical position, y (cm)	Velocity, u_x at 5 s (cm s^{-1})		Velocity, u_x at 20 s (cm s^{-1})		Velocity, u_x at 60 s (cm s^{-1})	
	Without surface tension	With surface tension	Without surface tension	With surface tension	Without surface tension	With surface tension
0.25	-2.28×10^{-5}	-2.17×10^{-5}	2.08×10^{-5}	1.73×10^{-5}	1.49×10^{-5}	1.11×10^{-5}
0.75	-3.74×10^{-5}	-3.60×10^{-5}	5.02×10^{-5}	4.30×10^{-5}	4.24×10^{-5}	4.46×10^{-5}
1.25	-3.52×10^{-5}	-3.38×10^{-5}	6.92×10^{-5}	5.97×10^{-5}	6.12×10^{-5}	5.31×10^{-5}
1.75	-3.52×10^{-5}	-3.37×10^{-5}	7.80×10^{-5}	6.73×10^{-5}	6.98×10^{-5}	5.0×10^{-5}
2.25	-4.06×10^{-5}	-3.87×10^{-5}	7.58×10^{-5}	6.47×10^{-5}	6.92×10^{-5}	5.85×10^{-5}
2.75	-5.48×10^{-5}	-5.28×10^{-5}	5.84×10^{-5}	4.85×10^{-5}	6.20×10^{-5}	6.38×10^{-5}
3.25	-8.62×10^{-5}	-8.37×10^{-5}	2.16×10^{-5}	1.53×10^{-5}	4.88×10^{-5}	4.87×10^{-5}
3.75	-1.15×10^{-4}	-1.10×10^{-4}	-3.68×10^{-5}	-3.48×10^{-5}	2.53×10^{-5}	1.08×10^{-5}
4.25	3.20×10^{-5}	3.22×10^{-5}	-1.15×10^{-4}	-9.78×10^{-5}	-8.76×10^{-5}	-8.09×10^{-5}
4.75	3.98×10^{-4}	3.78×10^{-4}	-2.22×10^{-4}	-1.83×10^{-4}	-2.96×10^{-4}	-2.60×10^{-4}
5.25	-3.52×10^{-1}	-3.73×10^{-1}	-1.46×10^{-3}	-1.60×10^{-3}	3.14×10^{-3}	1.53×10^{-3}
5.75	-2.08×10^{-1}	-2.11×10^{-1}	-5.68×10^{-2}	-5.02×10^{-2}	-2.96×10^{-2}	-2.78×10^{-2}
6.25	1.70×10^{-1}	1.63×10^{-1}	-3.50×10^{-2}	-2.60×10^{-2}	-4.44×10^{-2}	-4.0×10^{-2}
6.75	4.78×10^{-1}	4.78×10^{-1}	1.46×10^{-1}	1.37×10^{-1}	6.10×10^{-2}	5.99×10^{-2}
7.25	3.92×10^{-1}	4.02×10^{-1}	3.56×10^{-1}	3.38×10^{-1}	2.86×10^{-1}	2.78×10^{-1}
7.75	-3.90×10^{-1}	-3.71×10^{-1}	-7.88×10^{-2}	-6.82×10^{-2}	3.68×10^{-3}	7.14×10^{-3}
8.25	-1.73×10^{-1}	-1.72×10^{-1}	-1.41×10^{-1}	-1.37×10^{-1}	-1.19	-1.18
8.75	-2.64	-2.65	-2.50	-2.48	-2.30	-2.28
9.25	-9.46×10^{-1}	-9.64×10^{-1}	-1.05	-1.07	-1.01	-1.02
9.75	5.22	5.21	4.64	4.61	4.22	4.18

the velocity plots for the liquid phase for the case with surface tension is different from that for the case without surface tension. The important conclusion from the results discussed so far is that surface tension influences the flow when the gravity is reduced and when the temperature difference between the hot and cold walls is kept very high. The differences in the temperature along the interface for $Gr = 10^3$ and $g = 10^{-5}$ is as high as 18 K (at 60.0 s) as compared to 2.79 K and 0.9 K for $Gr = 10^6$ and 10^7, respectively. With higher Grashof number, the heat transport is convection dominated so that the surface temperature is more uniform. In the lower Grashof number case, the temperature is conduction dominated and greater surface temperature and surface-tension variations occur.

It is also observed that steady state occurs after about 60.0 s, and also that the results are not very much influenced by using the finer mesh size of 20 x 30, although the effect of surface tension at the interface can be better observed with this mesh.

A study is made of the effect of changing the

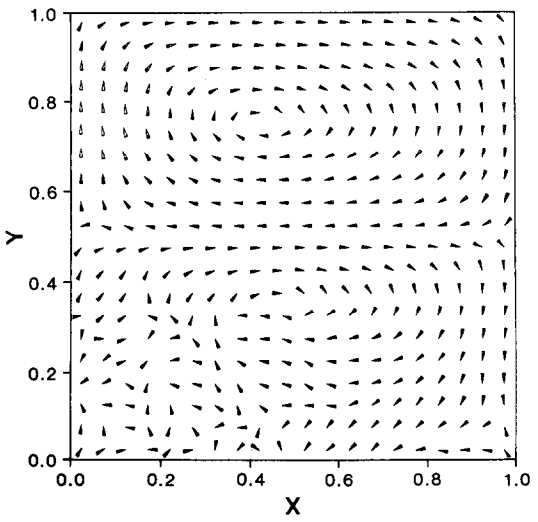

FIG. 12. $Gr = 10^3$, $h_1/h = 0.5$, velocity vector plots with surface tension, time: 60 s.

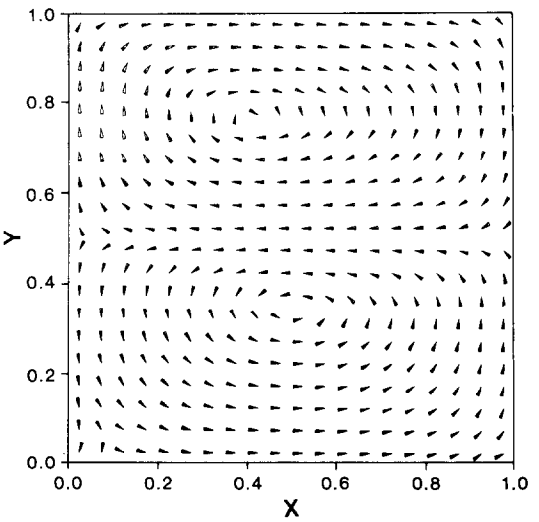

FIG. 13. $Gr = 10^3$, $h_1/h = 0.5$, velocity vector plots without surface tension, time: 60 s.

Table 3. Horizontal velocity profile at mid-radius. $Gr = 10^3$, $g = 10^{-5}$, $h_1/h = 0.5$, $A = 1$

Vertical position, y (cm)	Velocity, u_x at 5 s (cm s^{-1})		Velocity, u_x at 20 s (cm s^{-1})		Velocity, u_x at 60 s (cm s^{-1})	
	Without surface tension	With surface tension	Without surface tension	With surface tension	Without surface tension	With surface tension
0.25	3.43×10^{-8}	3.65×10^{-7}	5.83×10^{-7}	-4.77×10^{-5}	1.46×10^{-6}	-3.09×10^{-5}
0.75	5.25×10^{-8}	-2.01×10^{-7}	1.23×10^{-6}	-2.11×10^{-5}	3.41×10^{-6}	-1.21×10^{-5}
1.25	5.92×10^{-8}	-5.95×10^{-7}	1.59×10^{-6}	0.93×10^{-5}	4.52×10^{-6}	-1.51×10^{-4}
1.75	0.64×10^{-7}	-5.70×10^{-7}	1.80×10^{-6}	1.12×10^{-5}	4.90×10^{-6}	-1.37×10^{-4}
2.25	0.71×10^{-7}	-2.80×10^{-7}	1.88×10^{-6}	-0.95×10^{-5}	4.55×10^{-6}	-1.06×10^{-4}
2.75	0.77×10^{-7}	-1.43×10^{-8}	1.79×10^{-6}	-3.04×10^{-5}	3.39×10^{-6}	-7.16×10^{-5}
3.25	0.81×10^{-7}	1.13×10^{-7}	1.30×10^{-6}	-3.45×10^{-5}	1.26×10^{-6}	-2.29×10^{-5}
3.75	6.27×10^{-8}	1.42×10^{-7}	4.44×10^{-8}	-1.54×10^{-5}	-2.1×10^{-6}	5.93×10^{-5}
4.25	-4.16×10^{-8}	2.21×10^{-7}	-2.62×10^{-6}	3.02×10^{-5}	-7.06×10^{-6}	1.95×10^{-4}
4.75	-4.61×10^{-8}	7.81×10^{-7}	-7.62×10^{-6}	1.14×10^{-4}	-1.43×10^{-5}	3.99×10^{-4}
5.25	-2.12×10^{-4}	-2.78×10^{-4}	-1.29×10^{-3}	-2.63×10^{-3}	-1.62×10^{-3}	-3.15×10^{-3}
5.75	-4.04×10^{-4}	-4.51×10^{-4}	-2.65×10^{-3}	-3.35×10^{-3}	-3.32×10^{-3}	-4.14×10^{-3}
6.25	-4.61×10^{-4}	-4.66×10^{-4}	-3.0×10^{-3}	-3.22×10^{-3}	-3.74×10^{-3}	-4.04×10^{-3}
6.75	-4.23×10^{-4}	-3.94×10^{-4}	-2.50×10^{-3}	-2.40×10^{-3}	-3.09×10^{-3}	-3.02×10^{-3}
7.25	-3.01×10^{-4}	-2.62×10^{-4}	-1.37×10^{-3}	-1.04×10^{-3}	-1.62×10^{-3}	-1.29×10^{-3}
7.75	-0.88×10^{-4}	-5.85×10^{-5}	1.95×10^{-4}	0.64×10^{-3}	3.54×10^{-4}	0.85×10^{-3}
8.25	2.04×10^{-4}	2.21×10^{-4}	1.86×10^{-3}	2.34×10^{-3}	2.40×10^{-3}	2.96×10^{-3}
8.75	5.15×10^{-4}	5.25×10^{-4}	3.18×10^{-3}	3.61×10^{-3}	3.94×10^{-3}	4.49×10^{-3}
9.25	0.69×10^{-3}	7.01×10^{-4}	3.52×10^{-3}	3.84×10^{-3}	4.26×10^{-3}	4.68×10^{-3}
9.75	4.76×10^{-4}	4.81×10^{-4}	2.06×10^{-3}	2.21×10^{-3}	2.44×10^{-3}	2.63×10^{-3}

interface location by varying the ratio of the liquid height to cavity height (h_1/h). The aspect ratio is still fixed at unity. Results are obtained for both $Gr = 10^3$ and 10^8 with $g = 10^{-5}$ and 1.0, respectively. The temperature difference $(T'_w - T'_0)$ is kept at 1223 K. Two new sets of calculations are made for each of these Gr, with the cavity one-fourth filled ($h_1/h = 0.25$) and three-fourths filled ($h_1/h = 0.75$) with liquid.

From these results the following conclusions can be made about the effect of interface height: an increase in the liquid height results in an increased influence of the surface tension effect, especially at low gravity. For example with $Gr = 10^8$ and $g = 1.0$ there is very little influence of surface tension with all liquid heights, whereas at $Gr = 10^3$ and $g = 10^{-5}$ the influence on the flow is well observed at each height. Multicellular motion with higher Gr is observed in the gas phase for each height, whereas there is only one cell in the liquid phase even at $Gr = 10^8$. Thus surface tension clearly plays an important role in low gravity flows with greater liquid heights.

CONCLUDING REMARKS

Variations of five orders of magnitude in Grashof number were studied and significant differences were found in different parts of the range. As Grashof number increases, the number of circulatory cells in the gas phase increases. Furthermore, the magnitude of the gas and liquid velocities increase and the time to reach steady state decreases as Grashof number increases.

At high Grashof numbers such as 10^8, convective transport dominates and isotherms are close to horizontal. Also, augmentation by surface-tension-driven flows is not significant for the higher velocity portion of the gas. It has some effect in the liquid and in the bottom portion of the gas where the velocities are lower. This value of Grashof number is typical of an earth gravity environment with temperature variations of about 1000 K.

At low Grashof numbers such as 10^3, conductive transport dominates. This value is typical in a spacecraft environment. Augmentation of the buoyant flow by surface tension is extremely important as far as the velocity field is concerned; however, since convective transport is not important, surface tension does not have a major effect on the temperature field. The conclusion is, therefore, that surface tension does not affect the temperature field significantly at high or low Grashof numbers. Note that this study does not cover shallow enclosures. In such situations, buoyancy effects would be limited and temperature variations along the surface could be greater so that thermocapillary flows might significantly affect heat transport.

During the transient period, the nonuniform heating from above begins the circulatory motion with one cell caused by buoyancy. At higher Grashof numbers, more cells form with time in alternating directions of circulation on account of the reversal of the sign of the horizontal temperature gradient caused by the convective-dominated transport. As more cells form, the importance of convection in the lower cells diminishes since their Péclet number is decreased. This Péclet number decreases because: (1) the velocity in

the lower cells is less than in the upper cells; and (2) the characteristic length is less after more cells form. Once conduction becomes as important as convection in a lower cell, the horizontal component of the temperature gradient does not reverse its sign. Further cell development does not occur therefore after that point is reached.

Preliminary results with calculations at different aspect ratios show the same qualitative features.

As the interface height increases with constant total height of the enclosure, the number of cells in the gas phase decreased but the liquid motion remains unicellular. Note these calculations varied interface height at fixed Grashof number based upon total height. A Grashof number based upon gas height would, of course, decrease as interface height increases.

At low Grashof numbers, surface-tension effects become more important as interface height increases. Clearly, the temperature gradients along the surface increase as the surface moves closer to the heat source.

Effects of radiation, vaporization and mass transport, curvature of the surface, and changes of geometrical configurations should be included in future studies.

Acknowledgement—This research has been supported by a grant from NASA Lewis Research Center.

REFERENCES

1. S. Ostrach, Low-gravity fluid flows, *A. Rev. Fluid Mech.* **14**, 313–345 (1982).
2. W. A. Sirignano, A critical discussion of theories of flame spread across solid and liquid fuels, *Combust. Sci. Technol.* **6**, 95–105 (1972).
3. W. A. Sirignano and I. Glassman, Flame spreading above liquid fuels: surface-tension-driven flows, *Combust. Sci. Technol.* **1**, 307–312 (1970).
4. K. M. Torrance, Subsurface flows proceeding flame spread over a liquid fuel, *Combust. Sci. Technol.* **3**, 133 (1971).
5. C. W. Hirt, B. D. Nichols and N. C. Romero, SOLA—a numerical solution algorithm for transient fluid flows, Los Alamos Scientific Laboratory Report LA-5852 (April 1975).
6. H. Ozoe, H. Sayama and S. W. Churchill, Natural convection in an inclined rectangular channel at various aspect ratios and angles—experimental measurements, *Int. J. Heat Mass Transfer* **18**, 1425–1431 (1975).
7. I. Catton, A. Bejan, R. Grief and K. G. T. Hollands, Natural convection in enclosures, *Proc. Workshop on Natural Convection* (Edited by K. T. Yang and John R. Lloyd) (1982).
8. A. A. Emara and F. A. Kulacki, A numerical investigation of thermal convection in a heat-generating fluid layer, *J. Heat Transfer* **102**, 531–537 (1980).
9. S. Ostrach, R. R. Loka and A. Kumar, Natural convection in low aspect ratio rectangular enclosures, *Natural Convection in Enclosures* (Edited by K. Torrance and I. Catton), ASME HTD-8 (1980).

APPENDIX

The term N in the interface conditions is determined as follows:

$$\frac{NA}{Re^{1/2}} = \left|\frac{\partial\sigma}{\partial T}\frac{(T_w' - T_0')}{\mu_g'^{1/2}\rho_g'^{1/2}L'^{1/2}}\frac{1}{(u_{ref})^{3/2}}\right|.$$

With $NA/Re^{1/2} = 1$, we obtain

$$u_{ref} = \left[\left|\frac{\partial\sigma}{\partial T}\right|\frac{(T_w' - T_0')}{\mu_g'^{1/2}\rho_g'^{1/2}L'^{1/2}}\right]^{2/3}.$$

Note $NA \geqslant Re^{1/2}$ is stated when there is surface-tension dominance over buoyancy. Knowing u_{ref}, the Re_g and Gr/R_e^2 can be evaluated to study the effect of buoyancy. A sample calculation follows.

$$g' = 981\,\text{cm s}^{-2},\quad \beta = 0.33\times10^{-2}\,\text{K}^{-1}$$
$$H' = L' = 10\,\text{cm},\quad \rho_g' = 1.17\times10^{-3}\,\text{g cm}^{-3}$$
$$\nu_g' = 0.20\,\text{cm}^2\,\text{s}^{-1}\quad\text{and}\quad Gr = 10^5.$$

If we assume buoyancy dominates over surface tension, we state that

$$\frac{Gr}{R_e^2} = 1;$$

therefore $Re_g = 316$, and $u_{ref} = 6\,\text{cm s}^{-1}$. Suppose $T_w' - T_0' = 1.22\,\text{K}$.

$$\left|\frac{\partial\sigma}{\partial T}\right| = 0.10\quad\text{dynes cm}^{-1}\,\text{K}^{-1}$$

then

$$\frac{NA}{Re^{1/2}} = \left|\frac{0.1\times1.22}{(1.17\times10^{-3})\times(0.2)^{1/2}\times10^{1/2}}\frac{1}{(6.3)^{3/2}}\right|$$

$$\frac{NA}{Re^{1/2}} = 4.64.$$

This is a contradiction since $NA/Re^{1/2} > 1$ indicates surface-tension dominance. Therefore we now take

$$\frac{NA}{Re^{1/2}} = 1,$$

then

$$u_{ref} = 17\quad\text{cm s}^{-1}$$
$$Re_g = 854$$
$$\frac{Gr}{R_e^2} = 0.14.$$

This ratio indicates that the effect of surface tension is more important than the effect of buoyancy. Note that these estimates tend to overestimate the importance of surface tension since the hot wall temperature used in the calculation is much larger than the interface temperature.

GAZ ET LIQUIDE CONTENUS DANS UNE ENCEINTE ET CHAUFFES UNIFORMEMENT PAR DESSUS

Résumé—Les écoulements naturels de gaz surmontant un liquide dans une même enceinte, avec un chauffage non uniforme par dessus, sont étudiés en résolvant les équations par une méthode de différences finies. Des solutions variables sont calculées et les solutions stationnaires sont leurs formes asymptotiques. Des nombres de Grashof entre 10^3 et 10^8 sont considérés et la structure d'écoulement par circulation multicellulaire est trouvée pour les plus grands nombres de Grashof. Le transport convectif est dominant pour les plus grands nombres de Grashof tandis que le transport conductif est le mécanisme principal aux plus faibles nombres de Grashof. La tension interfaciale a un effet important sur le champ d'écoulement du gaz seulement pour les plus petits nombres de Grashof, mais puisque la conduction domine dans ce domaine elle n'affecte pas significativement le transport.

GAS UND FLÜSSIGKEIT IN EINEM GESCHLOSSENEN BEHÄLTER BEI UNGLEICHFÖRMIGER BEHEIZUNG VON OBEN

Zusammenfassung—In Gasen, welche sich zusammen mit Flüssigkeiten in von oben beheizten Behältern befinden, treten natürliche Konvektionsströmungen auf. Diese werden mit Hilfe eines Differenzenverfahrens untersucht. Transiente Lösungen werden berechnet und stationäre Lösungen asymptotisch angenähert. Der untersuchte Bereich umfaßt Grashof-Zahlen zwischen 10^3 und 10^8. Bei den größeren Grashof-Zahlen konnten multizellulare Strömungsstrukturen festgestellt werden. Konvektiver Wärmetransport dominiert im Bereich größerer Grashof-Zahlen, während für kleinere Grashof-Zahlen Wärmeleitung hauptsächlich zum Wärmetransport beiträgt. Die Oberflächenspannung hat nur bei kleineren Grashof-Zahlen einen gewissen Einfluß auf das Strömungsfeld des Gases. Da hier jedoch die Wärmeleitung dominiert, trägt sie nicht wesentlich zur Verbesserung des Wärmetransports bei.

НЕРАВНОМЕРНЫЙ НАГРЕВ СВЕРХУ ГАЗА И ЖИДКОСТИ В ЗАМКНУТОМ ОБЪЕМЕ

Аннотация—Конечно-разностными методами исследуются вызванные подъемными силами потоки в системе, образованной газом над жидкостью в общей полости, неравномерно нагреваемой сверху. Получены нестационарные решения, а стационарные представлены в виде асимптотик. Исследование выполнено при значениях числа Грасгофа в диапазоне от 10^3 до 10^8. При более высоких значениях этого числа поток приобретает характер многоячеечного циркуляционного течения. Конвективный перенос преобладает при более высоких числах Грасгофа, в то время как при более низких его значениях превалирует кондуктивный перенос. Поверхностное натяжение оказывает заметное влияние на поле скоростей газового потока только при низких числах Грасгофа, но поскольку при этом превалирует теплопроводность, существенного влияния на перенос оно не оказывает.